applied sciences

MDPI

Article

Drying Kinetics of Wheat (*Triticum aestivum* L., cv. 'Pionier') during Thin-Layer Drying at Low Temperatures

Iris Ramaj *, Steffen Schock and Joachim Müller

Tropics and Subtropics Group, Institute of Agricultural Engineering (440e), University of Hohenheim, 70599 Stuttgart, Germany; schock.steffen@uni-hohenheim.de (S.S.); joachim.mueller@uni-hohenheim.de (J.M.)
* Correspondence: i.ramaj@uni-hohenheim.de or info440e@uni-hohenheim.de; Tel.: +49-711-459-23119

Featured Application: Postharvest processing, low-temperature drying, aeration and cooling of in-store grain bulks, mathematical modeling.

Abstract: The management of moisture is one of the main challenges in anticipating and averting food decay and food losses during postharvest processing and storage. Hence, it is imperative to reduce the moisture of freshly harvested products to safe-storage limits in order to inhibit the occurrence of diverse biochemical, microbiological and other moisture-related deteriorative reactions which can contribute to quality degradation. A viable alternative to conventional hot-air drying is the application of low temperatures for drying, which has scarcely been investigated. In this regard, experimental-based modeling is a requisite to gain insights into drying processes. Thus, this study focused on investigating the drying kinetics of wheat (*Triticum aestivum* L.) cv. 'Pionier' under a coherent set of drying air temperatures (T = 10–50 °C), relative humidity (RH = 20–60%), and airflow velocity (v = 0.15–1.00 ms^{-1}). A robust and automated measurement system using a high precision balance was utilized as a basis for the real-time and continuous acquisition of drying data. The analysis of the experimental results facilitated the establishment of generalized drying model for low temperatures able to describe at a high accuracy the behavior of moisture ratio X^* (R^2 = 0.997, $RMSE$ = 1.285 × 10^{-2}, $MAPE$ = 6.5%). An analytical model for predicting the effective diffusion coefficients D (R^2 = 0.988, $RMSE$ = 4.239 × 10^{-2}, $MAPE$ = 7.7%) was also developed. In conclusion, the anticipated drying model has demonstrated the capability of modeling the drying behavior of wheat at low temperatures with a high temporal resolution and should be employed in the design, analysis and modeling of cooling, aeration and low-temperature drying processes of wheat bulks.

Keywords: wheat; aeration; cooling; low-temperature drying; high-precision dryer; modeling

Citation: Ramaj, I.; Schock, S.; Müller, J. Drying Kinetics of Wheat (*Triticum aestivum* L., cv. 'Pionier') during Thin-Layer Drying at Low Temperatures. *Appl. Sci.* **2021**, *11*, 9557. https://doi.org/10.3390/app11209557

Academic Editors: Malgorzata Nowacka, Urszula Tylewicz and Magdalena Dadan

Received: 17 September 2021
Accepted: 11 October 2021
Published: 14 October 2021

1. Introduction

Wheat is one of the major staple foods cultivated and consumed worldwide with an annual production quantity of 765.7 million metric tons in 2019 [1]. It is the second most-produced cereal worldwide after maize and accounts for nearly 28.6% of world cereal production. Wheat and its end-products are characterized by excellent organoleptic properties and stand as rich sources of carbohydrates, protein, vitamins, minerals, dietary fibers, and phytochemicals which are essential for human wellbeing and their nutritional balance [2,3]. However, when wheat is harvested at moisture contents above the safe level of 14% w.b., it is subjected to numerous biochemical, microbiological, and other moisture-related deteriorative reactions which can contribute to quality degradation [4,5]. Hence, a viable solution to counteract these problems is the application of low temperatures for cooling and drying which encompasses artificial aeration of grain with refrigerated air (ca. 10–20 °C), aeration with ambient air (ca. 20–35 °C), or low-temperature drying with additional heat supply (ca. 40–50 °C) [4,6–9]. These approaches allow grain to be retained within the safe limits for the occurrence of thermophilic insect attacks and mite infestation by avoiding the application of chemical agents [10,11]. During aeration, moisture is removed even at low temperatures, which in turn contributes to the inhibition of contaminant microorganisms such as fungi, yeasts, actinomycetes, and bacteria which are vulnerable to xerophilic conditions [4]. In contrast to high-temperature drying ($T > 50$ °C), low temperatures entail longer drying time due to the lower water vapor diffusivity in the drying product and lower water-uptake capacity of drying air [12]. However, the application of low temperatures for drying has proved to significantly enhance the quality retention of various agricultural products [13–15].

The conventional drying methods are commonly employed in practice as an easy-to-use approach that utilize high drying temperatures to obtain high drying rates [16,17]. Various drying methods such as convective drying [18], fluidized bed drying [19], cross-flow drying [20], mixed-flow drying [21] which apply high temperatures (T = 50–100 °C) for drying have been developed. Nevertheless, the high temperatures imparted to the grain during drying contribute to a series of undesirable changes in nutritional-functional properties such as denaturation of proteins, reduction of starch and nitrogen concentrations [22,23]; structural and textural properties such as transformation of starch granule sizes/shapes, damage of endosperm structure due to lower adhesion of starch granules and protein matrix, occurrence of kernels fissures and color changes [24,25]; cooking and sensory qualities of wheat end-products [26–28]. Henceforth, the application of low temperatures is a highly relevant alternative for rendering the grain safe from all risks and sustaining quality preservation [4,7].

However, drying remains an intricate process composed of simultaneous heat and moisture transfers. For this reason, the thin-layer models are used to provide an in-depth understanding of the air-product interaction and gain insights into drying processes. These models are analytical series solutions of the Fickian theory of diffusion and are essential for the process designing, and performance optimization. Several experimental-based models for describing the drying characteristics of wheat in thin-layers under specified laboratory conditions were employed in literature [29–33]. Nevertheless, substantial differences were observed among the developed models. An important factor having an effect may be the systems utilized for the acquisition of drying data. Discontinuous measurements using external balances or balances installed inside the test chambers have been employed, which may have potentially contributed to experimental errors or biased data [29,30,34]. Hence, robust and automated systems that ensure reliable and real-time acquisition of drying data using high precision balances should be adopted to lessen these effects [35,36]. Besides, different wheat varieties and/or harvest years were used to provide the empirical basis for the development of drying models [33,37]. The majority of models developed for describing the moisture transfer characteristics of wheat were carried out at temperatures of drying air from 30 to 70 °C [30,31,38–40]. However, the application of low temperatures has scarcely been investigated or constrained information was given in terms of drying conditions and their range of applicability [41,42].

Therefore, the objectives of this study were (i) to assess experimentally the drying behavior of wheat under a coherent set of low-temperature conditions applicable for cooling, aeration and drying of grain bulks, (ii) to characterize drying behavior using a semi-empirical modeling approach, and (iii) to establish a generalized drying model in which the drying air conditions are embodied in model parameters.

2. Materials and Methods

2.1. Raw Material and Sample Preparation

For this study, 100 kg of wheat (*Triticum aestivum* L.) cv. 'Pionier' (I.G. Pflanzenzucht GmbH, Ismaning, Germany), a representative high-quality cultivar in western Europe, was obtained from the Heidfeldhof experimental farm of University of Hohenheim, located in Stuttgart, Germany. A pneumatic conveyor was employed to remove the foreign substances such as dust, dirt, impurities as well as broken and immature kernels from the aggregate mass [43]. The moisture content was analyzed in triplicates using the thermogravimetric analysis in a convective oven (UM 700, Memmert GmbH & CO. KG, Schwabach, Germany) at 105 ± 1 °C for 24 h according to the AOAC [44]. The dried samples were cooled for 20 min in an airtight enclosure containing a desiccant substance and the final mass was measured via a laboratory balance (Sartorius BP221S, Sartorius AG, Göttingen, Germany) with an accuracy of ± 0.0001 g. An average moisture content of 0.159 ± 0.001 kg kg^{-1} d.b was observed. Afterwards, the wheat samples were remoistened to a level of 0.282 ± 0.015 kg kg^{-1} d.b. as described by Nimkar and Chattopadhyay [45] and Sacilik et al. [46] to increase the range of the envisaged drying curves. Thereafter, the samples were vacuum-sealed in transparent polyethylene (HDPE) bags of 500 g and stored in a refrigerator at 3.90 ± 0.28 °C for two weeks to guarantee uniform migration of moisture within kernels. Systematic visual inspections of samples for incidence of microbial growth were carried out during storage. After tempering, the samples were taken out to room temperature for 24 h to avert condensation prior to drying experiments. The principal dimensions length, width, and thickness of wheat kernels were measured using a Vernier caliper (Minutolo Co, Kawasaki, Japan) with a precision of ± 0.01 mm, and values of 6.12 ± 0.28, 3.50 ± 0.26, 3.13 ± 0.23 mm were observed accordingly.

2.2. Drying Experiments

Drying experiments were performed using a robust and automated system (HPD–TF1) designed at Institute of Agricultural Engineering, University of Hohenheim in Stuttgart, Germany. The CAD schematic design of the system is illustrated in Figure 1.

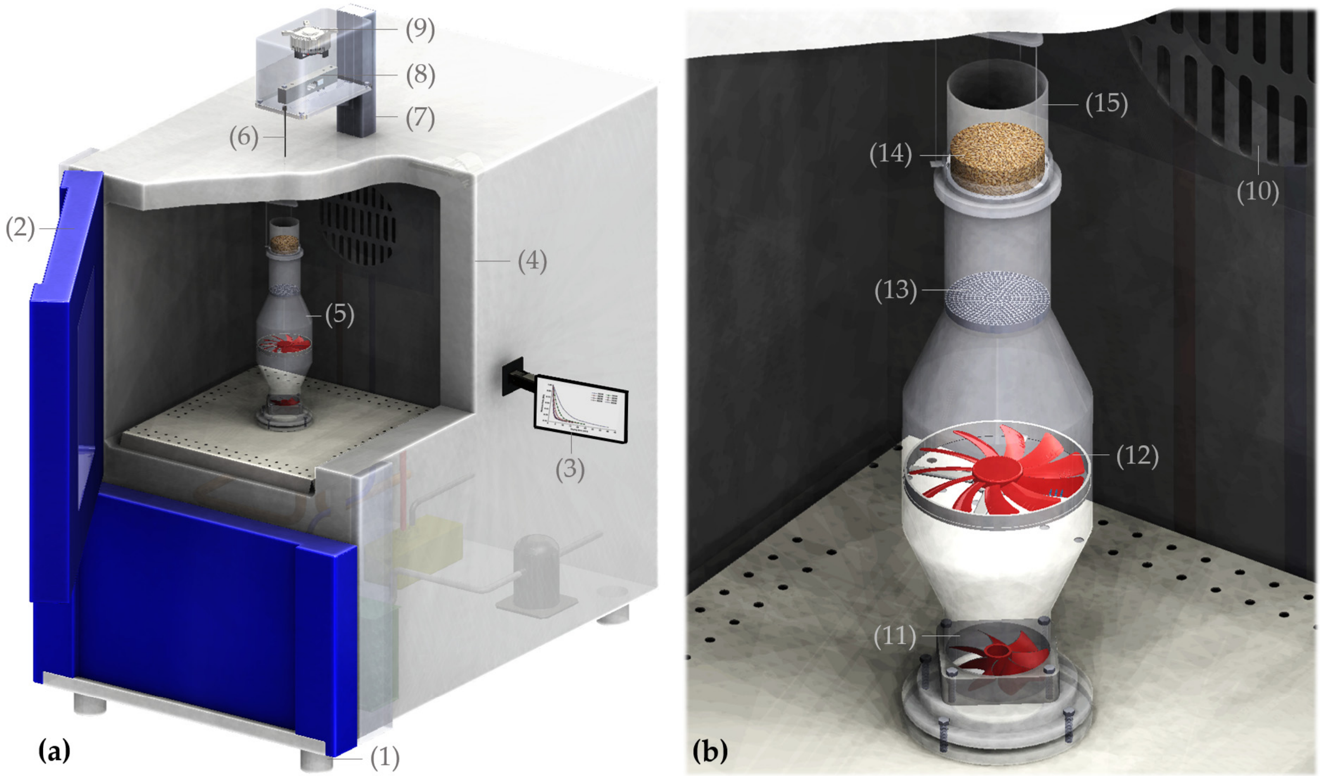

Figure 1. (**a**) Cutaway view of the automated drying system and (**b**) magnified view of the system interior; (1) vibration damping support, (2) mechanical door closer, (3) laboratory computer, (4) climatic test chamber, (5) drying column unit, (6) nylon string, (7) spindle drive, (8) load cell, (9) cooler, (10) air circulation fan, (11) axial fan, (12) vane anemometer, (13) airflow straightener, (14) thin-layer of wheat kernels, (15) acrylic sample holder.

The HPD–TF1 consisted of a climatic test chamber, a column drying unit and a weighing system. The drying air was conditioned through a climatic test chamber (CTS C-20/1000, CTS Clima Temperatur Systeme GmbH, Hechingen, Germany) with precise control of temperature (±0.1 °C) and relative humidity (±1.0%). Afterwards, the conditioned air was sucked by an axial fan (ebm-papst 8212J/2H4P, EBM-Papst Mulfingen GmbH & Co. KG, Mulfingen, Germany) through a column drying unit in a downwards direction. The corresponding air velocity was measured by means of a vane anemometer (Lambrecht 1468, Lambrecht meteo GmbH, Göttingen, Germany). In order to straighten the airflow and allow stable readings from the anemometer, an airflow straightener with a honeycomb configuration was employed. An automated and high-precision weighing system consisting of a load cell (AR 0.6 kg, Lorenz Messtechnik GmbH, Alfdorf, Germany) with a precision of ±0.02%, was mounted at the chamber ceiling. It allowed the sample holder (d = 70 mm, h =100 mm) to be suspended and weighed periodically during the drying experiments. At the bottom of the sample holder, a perforated floor (2 × 2 mm apertures) was used to allow the seamless flowing of drying air within the pore volume of kernels and hold them from falling. To prevent the buoyancy of air flow on the sample holder, the fan was stopped during the periodic weighing. The operating conditions and mass data were recorded in real-time and saved on a laboratory computer. A detailed portrayal of the system, its components, operating conditions, as well as measurement consistency, are described in-depth by Reyer et al. [47].

For the drying experiments, the conditions of the climatic chamber were set at temperatures T of 10, 20, 30, 40 and 50 °C, relative humidity RH of 20, 40 and 60% and airflow velocity v of 0.15, 0.50 and 1.00 ms^{-1}. The drying conditions are represented by codes such as *T30/RH40/V05*, which are ordered by T, RH and v, respectively. Prior to drying tests, the dryer was operated until the stability of set-conditions was reached. Afterwards, an aggregate mass of 85.41 ± 4.35 g of randomly selected wheat kernels was evenly loaded in the sample holder in a layer thickness of 0.04 m. The drying data were recorded at intervals of 720 s for a total of 1194.22 ± 239.63 min. At the end of each drying experiment, the final moisture content was re-analyzed using the thermogravimetric analysis. Each drying test was carried out in triplicates and for the drying characteristics, the mean values of the experimental moisture content were used. The equilibrium moisture content of wheat was assessed experimentally using the gravimetric salt method as described by Udomkun et al. [48]. Temperatures of 10, 30 and 50 °C and 8 sets of relative humidity produced from the saturated salt solutions ranging from 12.3 to 86.8% were used for the determination of the equilibrium moisture content X_{eq}. A laboratory balance (Sartorius BP221S, Sartorius AG, Göttingen, Germany) was employed to measure the changes in the weight with an accuracy of ±0.0001 g. The equilibrium state was deemed once these changes were less than 0.1% in the last three consecutive measurements. The experiments were carried out in triplicates. The Modified Oswin model was used to fit X_{eq} from experimental data, as shown in Equation (1).

$$X_{eq} = (C_1 + C_2 T)\left(\frac{RH/100}{1 - RH/100}\right)^{1/C_3} \tag{1}$$

where X_{eq} (kg kg^{-1} d.b.) is the equilibrium moisture content, T (°C) is the temperature of air, RH (%) is the relative humidity of air and C_1, C_2 and C_3 are the model coefficients.

2.3. Modeling of Drying Behavior

From the acquisition of drying data, moisture ratio X^* and drying rate $dXdt^{-1}$ were calculated as follows:

$$X^* = \frac{X_t - X_{eq}}{X_0 - X_{eq}} \tag{2}$$

$$\frac{dX}{dt} = \frac{X_t - X_{t+\Delta t}}{\Delta t} \tag{3}$$

where X^* is the moisture ratio, X_t (kg kg^{-1} d.b.) is the instantaneous moisture content at time t during drying, $X_{t+\Delta t}$ (kg kg^{-1} d.b.) is initial moisture content at time t + Δt, t (min) is the drying time and Δt (min) is the time difference. The calculations for Equations (2) and (3) were performed stepwise for the measuring interval. Afterwards, the experimentally observed data of moisture ratio and drying time was fitted using the semi-empirical models given in Table 1 [49–53]. These models are derived as simplification forms of the general series solution of Fickian moisture transport theory which require less assumptions in contrast to the theoretical models [54–56]. However, semi-empirical models offer a decent compromise between the physical theory and ease of use [54]. From Table 1, k (min^{-1}) is the drying constant and A_0, A_1, n are the empirical coefficients of drying models. The perceived drying constant and/or coefficients from the best-fitting model were used to develop generalized models in relation to the drying conditions (temperature T, relative humidity RH, airflow velocity v) via a nonlinear regression analysis as described by Udomkun et al. [57] and Munder, Argyropoulos and Müller [36].

Table 1. Moisture ratio (X^*) and drying rate ($dXdt^{-1}$) expressions obtained from the semi-empirical models employed for modeling the drying behavior of wheat cv. 'Pionier'.

Model	Expression	Equation	Expression	Equation
Newton	$X^* = e^{-kt}$	(4)	$dXdt^{-1} = -ke^{-kt}$	(5)
Page	$X^* = e^{-kt^n}$	(6)	$dXdt^{-1} = -knt^{n-1}e^{-kt^n}$	(7)
Henderson	$X^* = A_0e^{-kt}$	(8)	$dXdt^{-1} = -kA_0e^{-kt}$	(9)
Ademiluyi	$X^* = A_0e^{-kt^n}$	(10)	$dXdt^{-1} = -kA_0nt^{n-1}e^{-kt^n}$	(11)
Logarithmic	$X^* = A_0\, e^{-kt} + A_1$	(12)	$dXdt^{-1} = -ke^{-kt}$	(13)
Midili	$X^* = A_0\, e^{-kt} + A_1t$	(14)	$dXdt^{-1} = -ke^{-kt} + A_1$	(15)
Peleg	$X^* = 1 - t/(A_0 + A_1t)$	(16)	$dXdt^{-1} = -A_0/(A_0 + A_1t)^2$	(17)
Weibull	$X^* = e^{-(t/A_0)^{A_1}}$	(18)	$dXdt^{-1} = -\left(A_0(t/A_0)^{A_0}\, e^{-(t/A_0)^{A_1}}\right)/t$	(19)

2.4. Analytical Estimation of Moisture Diffusion Coefficients

During drying process, diffusion is assumed to be a complex mechanism which transfers the internal moisture towards the surface of the product. With a lumped parameter model concept, all its phenomena are combined in one term named effective moisture diffusivity which remains constant for sufficiently long drying time [36,55]. Based on assumption of spherical, homogeneous and isotropic wheat kernels, negligible volumetric shrinkage, unidimensional moisture removal, and constant moisture diffusion during drying, the long times analytical solution of diffusion equation is expressed as [58]:

$$X^* = \frac{X_t - X_{eq}}{X_0 - X_{eq}} = \frac{6}{\pi^2}\sum_{i=1}^{N}\frac{1}{N^2}e^{\left(-n^2\pi^2\frac{Dt}{R_e^2}\right)} \tag{20}$$

where D (m^{2}s^{-1}) is the effective moisture diffusion coefficient and R_e (m) is the equivalent radius of the wheat kernel. The infinite series have been simplified by Giner and Mascheroni [59] without losing the accuracy and physical meaning. The simplified analytical solution of the diffusion equation for short times has a range of applicability ($1 \leq X^* \leq 0.2$) corresponding to the fast-drying phase. It is based on the assumption that changes in moisture are constrained to the vicinity of the surface. Hence, the analytical solution for short times is expressed as:

$$X^* = 1 - \frac{2}{\sqrt{\pi}}\alpha_v\sqrt{Dt} + 0.331{\alpha_v}^2Dt \tag{21}$$

where α_v (m^{2}m^{-3}) is the kernel-specific surface area. The kernel-specific surface area ($\alpha_v = 6/d_e$) is determined based on the kernel equivalent diameter ($d_e = 4.06 \pm 0.21$ mm) according to Giner and Mascheroni [30].

2.5. Statistical Analysis

Software SAS 9.4 (SAS Inst., Cary, NC, USA) was used to perform the analysis of variance (ANOVA). The graphical presentation and fitting of drying data were carried out using the nonlinear least-squares solver of curve fitting toolbox of MATLAB 2019a (MathWorks Inc., Natick, MA, USA) at the significance level of 95% ($p \leq 0.05$). The coefficient of determination R^2, the root means square error $RMSE$ and mean absolute percentage error *MAPE* were used to assess statistically the goodness of fit based on the observed X^*_{exp} and predicted X^*_{pred} moisture ratio for N observations [55].

$$R^2 = 1 - \left(\frac{\sum_{i=1}^{N} \left(X^*_{exp} - X^*_{pred} \right)^2}{\sum_{i=1}^{N} \left(X^*_{exp} - \overline{X^*_{exp}} \right)^2} \right) \quad (22)$$

$$RMSE = \sqrt{\frac{\sum_{i=1}^{N} \left(X^*_{exp} - X^*_{pred} \right)^2}{N}} \quad (23)$$

$$MAPE = \frac{100}{N} \sum_{i=1}^{N} \left| \frac{X^*_{exp} - X^*_{pred}}{X^*_{exp}} \right| \quad (24)$$

The same statistical indicators were used to evaluate the quality of fit for equilibrium moisture content X_{eq} and drying constant k. A sensitivity analysis by MATLAB/Simulink 2019a (MathWorks Inc., Natick, MA, USA) was utilized to test the effect of drying conditions on drying behavior. The standardized regression coefficients were reported accordingly.

3. Results and Discussion

3.1. Equilibrium Moisture Content

Figure 2 presents the experimentally observed data of the equilibrium moisture content X_{eq} depending on temperature T and relative humidity RH of the surrounding air and fitted curves predicted from the Modified Oswin model. Results demonstrated a decrease of moisture content X_{eq} as the temperature of the surrounding air increases at a given constant relative humidity, implying less hygroscopic capacity due to structural changes induced by temperatures and increased excitation of water molecules breaking off from the product. Moreover, at a constant temperature the moisture content X_{eq} increased with the increment of the relative humidity and experienced a large degree of upturn at $RH > 85\%$ [54,60].

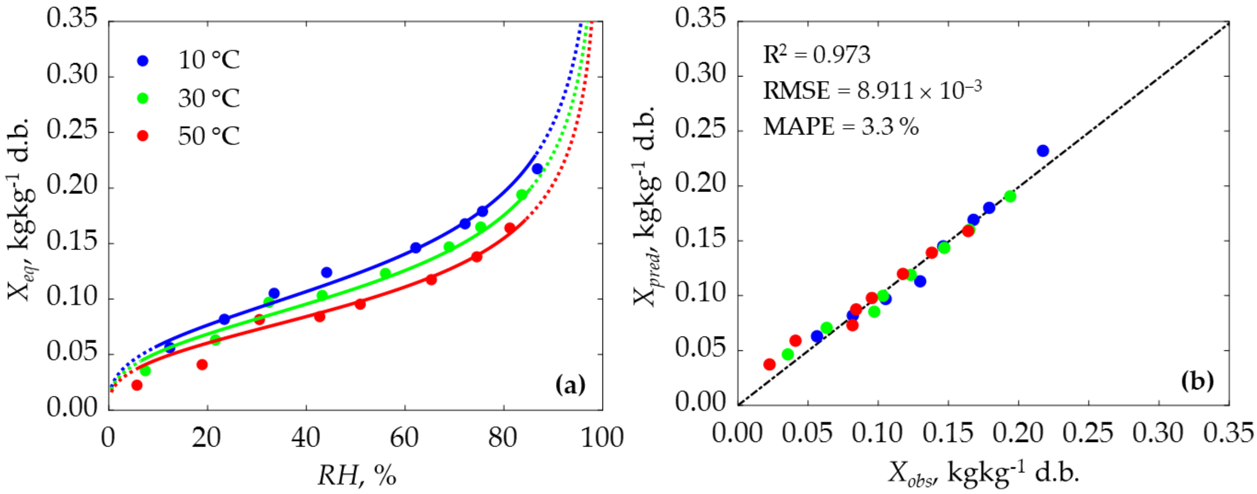

Figure 2. (**a**) Sorption isotherm for wheat cv. 'Pionier' at 10, 30, and 50 °C. Dashed lines reflect extrapolations beyond the dataset used for fitting; (**b**) scatter plot of predicted X_{pred} versus observed moisture content X_{obs}.

The experimentally observed data matched the characteristic sigmoid relationship type-II sorption isotherm based on the categorization of Brunauer [61] for biological and food materials. From the analysis of variance, both the relative humidity RH and temperature T were found to significantly affect the changes of equilibrium moisture content X_{eq} at $p \leq 0.05$. The mean values of X_{eq} and corresponding standard deviations among the replicates for all sets of temperature and relative humidity are summarized in Appendix A. The fitting analysis revealed that the Modified Oswin model (Equation 1) was able to predict the relationship of X_{eq} with T and RH with an accuracy of R^2 = 0.973, $RMSE$ = 8.911 × 10^{-3} and $MAPE$ = 3.3% in the range of applicability of 10 ≤ T ≤ 50 °C and 5.7 ≤ RH ≤ 86.8%. The empirical coefficients derived from the fitting analysis were C_1 = 0.129, C_2 = −6.460 × 10^{-4} and C_3 = 2.944, respectively. The relationship between the predicted and observed X_{eq} is shown graphically in Figure 2b. The data were dispersed around the straight line (X_{pred} = X_{obs}), indicating a high prediction from the employed model.

3.2. Evaluation of the Drying Models

The drying data measured in each drying setting were converted into the moisture ratio X^* and then the moisture ratio as a function of drying time was fitted by the semi-empirical models given in Table 1. Table 2 presents a summary of the drying constant k, empirical coefficients n, A_0 and A_1, as well as the coefficient of determination R^2, root means square error $RMSE$ and mean absolute percentage error $MAPE$ acquired from individual fittings at each drying condition. The inspection of the statistical indicators showed that the employed models had the capability to depict the drying behavior of wheat cv. 'Pionier' with an R^2, $RMSE$ and $MAPE$ ranging from 0.948 to 0.999, 5.514 × 10^{-3} to 5.021 × 10^{-2} and 1.2 to 37.1%. The selection of the most suitable model was determined based on the statistical criteria [55]. From the analysis of Table 2 it was revealed that increase of the complexity of the model and numbers of terms did not meaningfully improve the fit accuracy. Hence, the Page model was selected as the most suitable model to fit the experimental data with the statistical indicators R^2 ranging from 0.995 to 0.999, $RMSE$ ranging from 7.608 × 10^{-3} to 1.559 × 10^{-2} and $MAPE$ from 1.2 to 18.2%, which assured high accuracy of prediction by maintaining an acceptable level of complexity. The model revealed the capability to accurately describe the drying kinetics for temperatures above 30 °C, which stands in line with literature [33,38]. This study demonstrated that the Page model also can be used to predict with a high accuracy (R^2 ≥ 0.997, $RMSE$ ≤ 1.193 × 10^{-2} and $MAPE$ ≤ 4.6%) the drying behavior of wheat subjected to low-temperature ranges of 10–30 °C, which has scarcely been investigated to date. Thereby, it gave the opportunity for the creation of a generalized drying model that allows characterization of wheat drying kinetics under a coherent set of low temperatures (T = 10–50 °C) suitable for cooling, aeration, and drying of wheat. Moreover, the Page model proved to be effective in predicting the drying behavior for different relative humidities and velocities of drying air applied in this study.

3.3. Drying Characteristics

Figure 3a displays the drying characteristics of wheat at T ranging from 10 to 50 °C, whereas maintaining the RH and v at fixed values of 40% and 0.15 ms^{-1}. The X_{eq} was calculated from the Modified Oswin model for T of 10, 20, 30, 40 and 50 °C where values of 0.107, 0.101, 0.096, 0.090 and 0.084, were observed, respectively. From the inspection of Figure 3a, for all temperatures the data of X^* exhibited a decreasing rate with the drying time t with the increment of T. Significant differences were observed among drying kinetics at $p \leq 0.05$. At the inception of drying (t < 400 min), the course of X^* is characterized by a steep drying gradient ascribed to superficial moisture removal, which accelerated the drying process. At $t \geq 400$ min, a descent and downward gradient was observed.

Table 2. Summary of drying constant k, coefficients n, A_0, A_1, coefficient of determination R^2, root means square error $RMSE$ and mean absolute percentage error $MAPE$ observed from fitting of semi-empirical models with the experimental data.

Code	Model Parameters, Statistical Indicators	Newton	Page	Henderson	Ademiluyi	Logarithmic	Midili	Peleg	Weibull
T10/RH40/V015	k, min^{-1}	8.657×10^{-4}	4.380×10^{-3}	7.497×10^{-4}	4.168×10^{-3}	1.239×10^{-3}	9.941×10^{-3}	–	–
	n, –	–	0.757	–	0.763	–	–	–	–
	A_0, –	–	–	0.922	0.993	0.724	0.949	784.2	1309
	A_1, –	–	–	–	–	0.229	8.685×10^{-5}	1.006	0.757
	R^2, –	0.954	0.998	0.988	0.998	0.994	0.994	0.994	0.998
	$RMSE$, –	3.581×10^{-2}	7.833×10^{-3}	1.819×10^{-2}	7.846×10^{-3}	1.277×10^{-2}	1.348×10^{-2}	1.361×10^{-2}	7.833×10^{-3}
	$MAPE$, %	5.3	1.2	2.2	1.2	1.8	1.8	2.1	1.2
T20/RH40/V015	k, min^{-1}	1.612×10^{-3}	5.471×10^{-3}	1.449×10^{-3}	5.505×10^{-3}	1.965×10^{-3}	1.755×10^{-3}	–	–
	n, –	–	0.811	–	0.810	–	–	–	–
	A_0, –	–	–	0.917	1.001	0.849	0.952	439.3	616.9
	A_1, –	–	–	–	–	0.108	6.067×10^{-5}	0.859	0.811
	R^2, –	0.976	0.999	0.992	0.999	0.999	0.998	0.998	0.999
	$RMSE$, –	3.400×10^{-2}	7.608×10^{-3}	1.983×10^{-2}	7.642×10^{-3}	8.700×10^{-3}	9.240×10^{-3}	9.466×10^{-3}	7.608×10^{-3}
	$MAPE$, %	9.0	2.1	5.1	2.1	1.6	1.6	2.2	2.1
T30/RH40/V015	k, min^{-1}	2.323×10^{-3}	9.502×10^{-3}	2.047×10^{-3}	1.246×10^{-2}	2.945×10^{-3}	2.571×10^{-3}	–	–
	n, –	–	0.774	–	0.736	–	–	–	–
	A_0, –	–	–	0.896	1.040	0.864	0.951	274.4	411.2
	A_1, –	–	–	–	–	0.097	6.707×10^{-5}	0.883	0.774
	R^2, –	0.964	0.997	0.982	0.998	0.998	0.997	0.999	0.997
	$RMSE$, –	4.286×10^{-2}	1.193×10^{-2}	3.078×10^{-2}	1.039×10^{-2}	9.684×10^{-3}	1.230×10^{-3}	7.614×10^{-3}	1.193×10^{-2}
	$MAPE$, %	18.7	4.6	12.5	3.8	3.1	4.1	3.0	4.6
T40/RH40/V015	k, min^{-1}	5.037×10^{-3}	1.566×10^{-2}	4.538×10^{-3}	1.879×10^{-2}	5.779×10^{-3}	5.243×10^{-3}	–	–
	n, –	–	0.794	–	0.766	–	–	–	–
	A_0, –	–	–	0.911	1.033	0.909	0.952	123.2	188.2
	A_1, –	–	–	–	–	0.055	6.151×10^{-5}	0.898	0.794
	R^2, –	0.975	0.995	0.984	0.996	0.999	0.998	0.994	0.995
	$RMSE$, –	3.562×10^{-2}	1.559×10^{-2}	2.911×10^{-2}	1.494×10^{-2}	6.810×10^{-3}	1.000×10^{-2}	1.736×10^{-2}	1.559×10^{-2}
	$MAPE$, %	34.0	13.9	27.4	6.4	3.6	11.3	13.1	13.9
T50/RH40/V015	k, min^{-1}	1.070×10^{-2}	2.193×10^{-2}	1.012×10^{-3}	2.424×10^{-2}	1.151×10^{-2}	1.081×10^{-2}	–	–
	n, –	–	0.849	–	0.832	–	–	–	–
	A_0, –	–	–	0.950	1.019	0.947	0.969	58.3	90.11
	A_1, –	–	–	–	–	0.030	5.744×10^{-5}	0.898	0.849
	R^2, –	0.989	0.997	0.992	0.997	0.992	0.998	0.991	0.997
	$RMSE$, –	2.318×10^{-2}	1.254×10^{-2}	2.075×10^{-2}	1.228×10^{-2}	6.450×10^{-3}	9.260×10^{-3}	2.247×10^{-2}	1.254×10^{-2}
	$MAPE$, %	37.1	18.2	32.6	17.3	6.6	9.1	22.1	18.2

Table 2. *Cont.*

Code	Model Parameters, Statistical Indicators	Newton	Page	Henderson	Ademiluyi	Logarithmic	Midili	Peleg	Weibull
T30/RH20/V015	k, min^{-1}	2.600×10^{-3}	7.901×10^{-3}	2.350×10^{-3}	8.847×10^{-3}	2.873×10^{-3}	2.654×10^{-3}	–	–
	n, –	–	0.819	–	0.803	–	–	–	–
	A_0, –	–	–	0.912	1.016	0.895	0.942	262.8	368.4
	A_1, –	–	–	–	–	0.055	3.659×10^{-5}	0.857	0.819
	R^2, –	0.981	0.999	0.992	0.999	0.997	0.997	0.999	0.999
	$RMSE$, –	3.214×10^{-2}	5.510×10^{-2}	2.131×10^{-2}	5.002×10^{-2}	1.194×10^{-3}	1.340×10^{-2}	5.514×10^{-2}	5.550×10^{-3}
	$MAPE$, %	17.4	2.6	10.5	2.5	4.9	5.3	3.4	2.6
T30/RH60/V015	k, min^{-1}	2.072×10^{-3}	9.077×10^{-3}	1.814×10^{-3}	1.156×10^{-2}	2.755×10^{-3}	2.354×10^{-3}	–	–
	n, –	–	0.764	–	0.731	–	–	–	–
	A_0, –	–	–	0.895	1.033	0.835	0.950	309.2	469.6
	A_1, –	–	–	–	–	0.125	8.626×10^{-5}	0.903	0.764
	R^2, –	0.959	0.998	0.982	0.999	0.998	0.997	0.999	0.998
	$RMSE$, –	4.441×10^{-2}	9.974×10^{-3}	2.985×10^{-2}	8.636×10^{-3}	1.054×10^{-2}	1.275×10^{-2}	5.760×10^{-3}	9.974×10^{-3}
	$MAPE$, %	14.1	2.8	8.5	2.3	2.6	3.1	1.7	2.8
T30/RH40/V05	k, min^{-1}	2.392×10^{-3}	1.201×10^{-3}	2.054×10^{-3}	1.675×10^{-2}	3.182×10^{-3}	2.696×10^{-3}	–	–
	n, –	–	0.740	–	0.694	–	–	–	–
	A_0, –	–	–	0.877	1.054	0.849	0.944	251.1	395.0
	A_1, –	–	–	–	–	0.110	7.738×10^{-5}	0.918	0.740
	R^2, –	0.948	0.996	0.973	0.997	0.998	0.996	0.999	0.996
	$RMSE$, –	5.021×10^{-2}	1.418×10^{-2}	3.643×10^{-2}	1.197×10^{-2}	1.111×10^{-2}	1.497×10^{-2}	6.566×10^{-3}	1.418×10^{-2}
	$MAPE$, %	22.2	5.4	14.7	4.4	3.8	5.3	2.4	5.4
T30/RH40/V1	k, min^{-1}	2.656×10^{-3}	1.237×10^{-3}	2.292×10^{-3}	1.682×10^{-2}	3.367×10^{-3}	2.893×10^{-3}	–	–
	n, –	–	0.748	–	0.706	–	–	–	–
	A_0, –	–	–	0.880	1.052	0.864	0.940	228.7	353.9
	A_1, –	–	–	–	–	0.093	6.559×10^{-5}	0.909	0.748
	R^2, –	0.954	0.996	0.975	0.997	0.996	0.994	0.999	0.996
	$RMSE$, –	4.784×10^{-2}	1.406×10^{-2}	3.537×10^{-2}	1.209×10^{-2}	1.416×10^{-2}	1.814×10^{-2}	7.081×10^{-3}	1.406×10^{-2}
	$MAPE$, %	25.0	5.6	16.8	4.2	7.1	8.6	2.2	5.3

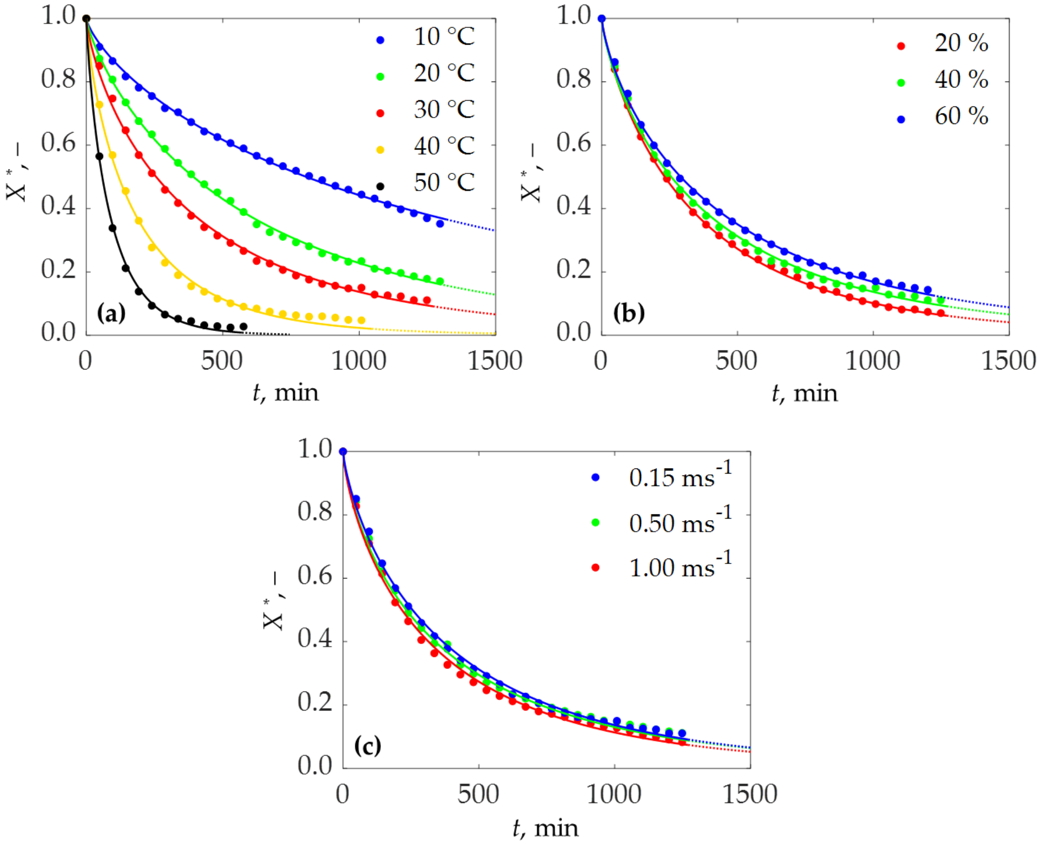

Figure 3. Moisture ratio X^* vs. time t; (**a**) temperature T ranging from 10 to 50 °C at relative humidity RH = 40%, airflow velocity v = 0.15 ms^{-1}; (**b**) RH ranging from 20 to 60% at T = 30 °C, v = 0.15 ms^{-1}; (**c**) v ranging from 0.15 to 1.00 ms^{-1} at T = 30 °C, RH = 40%. Solid lines represent Page model fitting, dashed lines show extrapolation beyond the dataset used for fitting.

This behavior can be accredited to the lower thermal conductivity and increased resistance of the internal moisture migration towards the wheat kernel surface, leading to the reduction in drying rates [57]. However, a flatter course was experienced for temperatures 10 and 20 °C leaning towards the X_{eq} compared to other temperatures. These results were in line with the literature, especially for $T \geq 30$ °C [30,31,33]. However, there is limited information available in the literature on temperatures below 30 °C.

The time required to reduce the X^* from 1 to 0.350 is compared, where 1320, 624, 420, 204, 96 min of drying were observed when drying at temperatures 10, 20, 30, 40, 50 °C, respectively. Therefore, a decrease of 92.7% in drying time t was observed when increasing T from 10 to 50 °C. From Table 2, the Page model fitted the experimental data at a high accuracy with the R^2 ranged from 0.995 to 0.999, $RMSE$ from 7.608×10^{-3} to 1.559×10^{-3} and $MAPE$ from 1.1 to 18.2%. The k values comprised between 4.380×10^{-3} and 2.193×10^{-2}, whereas n values were between 0.757 and 0.849. The fitted drying curves presented a good fitting with the experimental data followed by a slight underestimation at the end of drying, particularly at 40 and 50 °C which can be attributed to a minor difference between the final moisture at equilibrium state attained from the drying system and the equilibrium X_{eq} predicted from Equation (1).

In addition, Figure 3b shows the course of X^* affected by RH ranging from 20 to 60% at temperature T = 30 °C and airflow velocity v = 0.15 ms^{-1}. The values of X_{eq} were 0.068, 0.096 and 0.126 for 20, 40 and 60% of RH, respectively. Results indicated that the increase of RH, decreased X^* with the drying time t which was in line with the outcomes of Jayas and Sokhansanj [62]. In contrast, they disagreed with the findings of Singh, Sokhansanj and Middleton [42] who stated that RH does not affect the drying characteristics of wheat.

This can be ascribed to the higher water-holding capacity of air at low *RH*, which causes the speeding-up of the moisture transfer over the same drying time.

Precisely, the increment of *RH* from 20 to 60%, decreases the absolute humidity of drying air from 5.270×10^{-3} to 1.608×10^{-2} and saturation deficit from 5.800×10^{-3} to 2.550×10^{-4}. In this regard, a shorter *t* of about 28.1% is required to reach a target X^* = 0.350 when decreasing the *RH* from 60 to 20% at the same *T* and *v*. Nevertheless, the influence of the *RH* was noticeably smaller compared to the *T* effect. A high prediction was observed by the Page model (R^2 = 0.997–0.999, *RMSE* = 5.510×10^{-3}–1.119×10^{-2}, *MAPE* = 2.6–4.6%). The *k* values comprised between 7.901×10^{-3} and 9.502×10^{-3}, whereas *n* values were falling between 0.764 and 0.819.

Moreover, the effect of *v* on X^* is illustrated in Figure 3c. The *v* varied from 0.15 to 1.00 ms^{-1}, while *RH* = 40% and *T* = 30 °C. The results indicated that the increase of *v* exhibited a faster reduction of X^*, which may be attributed to the faster heat transfer between the drying air and kernels, hence favored a more rapid drying process. The air velocity acted as an agent for supplying heat to kernels via convection and enabled the acceleration of moisture evaporation. At *v* =1.00 ms^{-1}, the time required to reach a target X^*= 0.350 was 348 min compared to 420 min needed for *v* = 0.15 ms^{-1}, which resulted in a reduction of 17.1%. However, it remains evident, that *v* had the least effect on the drying behavior compared to *T* and *RH*. Alike findings were reported by Watson and Bhargava [34] and Cao and Yu [39] who agreed that *v* has a minor impact on the drying behavior of wheat. The statistical indicators revealed that the fitting model accurately anticipated the drying data at different *v*. Particularly, the $R^2 \geq 0.996$, *RMSE* $\leq 1.418 \times 10^{-2}$ and *MAPE* $\leq$ 5.6%. The values of *k* and *n* ranged from 9.502×10^{-3} to 1.237×10^{-2} and from 0.740 to 0.774.

Figure 4a presents the distribution of the residuals in a histogram chart computed as the difference between observed X^*_{obs} and predicted X^*_{pred} by Page model. The distribution of the residuals was soundly symmetric and unimodal around the abundant value 0 and suggesting a fairly normal distribution, which supported the validity of the selected model. The residuals were randomly scattered between −0.045 and 0.025. However, the majority of residuals (frequency from 31.86 to 34.13%) fell between 1.667×10^{-3} and 7.50×10^{-3}. The observed versus predicted plot in Figure 4b displays a closely straight-line distribution of data which signposts a high accuracy prediction with R^2 = 0.998, *RMSE* = 1.110×10^{-2} and *MAPE* = 5.8%.

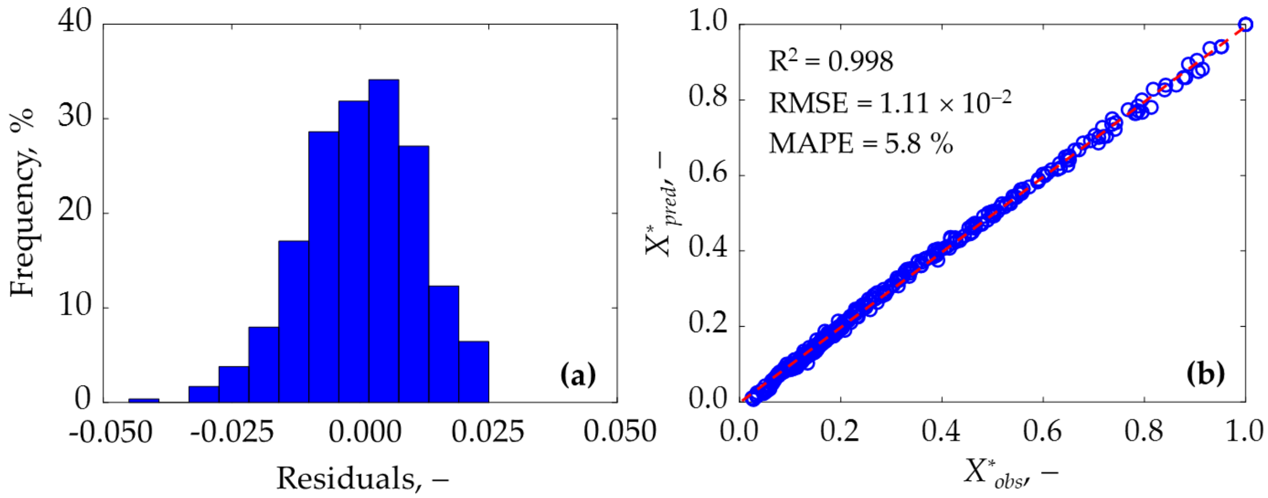

Figure 4. (**a**) Frequency distribution of residuals; (**b**) observed moisture ratio X^*_{obs} vs. predicted X^*_{pred} for all sets of drying conditions.

Moreover, the variation of the drying rate $dXdt^{-1}$ over drying time *t* for the selected drying conditions is shown graphically in Figure 5. Overall, the highest changes of $dXdt^{-1}$ were observed within the time-period (*t* < 400 min), where the migration of a large amount of moisture occurred. Afterwards, a progressive decrease over a more extended period was observed which can be ascribed to the greater internal resistance for water removal. The maximum values ranged from 2.678×10^{-4} to 2.426×10^{-3} kg kg^{-1} min^{-1} for T from 10 to 50 °C, 9.087×10^{-4} to 6.449×10^{-4} kg kg^{-1} min^{-1} for RH from 20 to 60%, 6.732×10^{-4} to 8.526×10^{-4} kg kg^{-1} min^{-1} for v from 0.15 to 1.00 ms^{-1}, respectively. In analogy with X^*, the T was the more profound parameter which affected the drying rate, followed by RH and v.

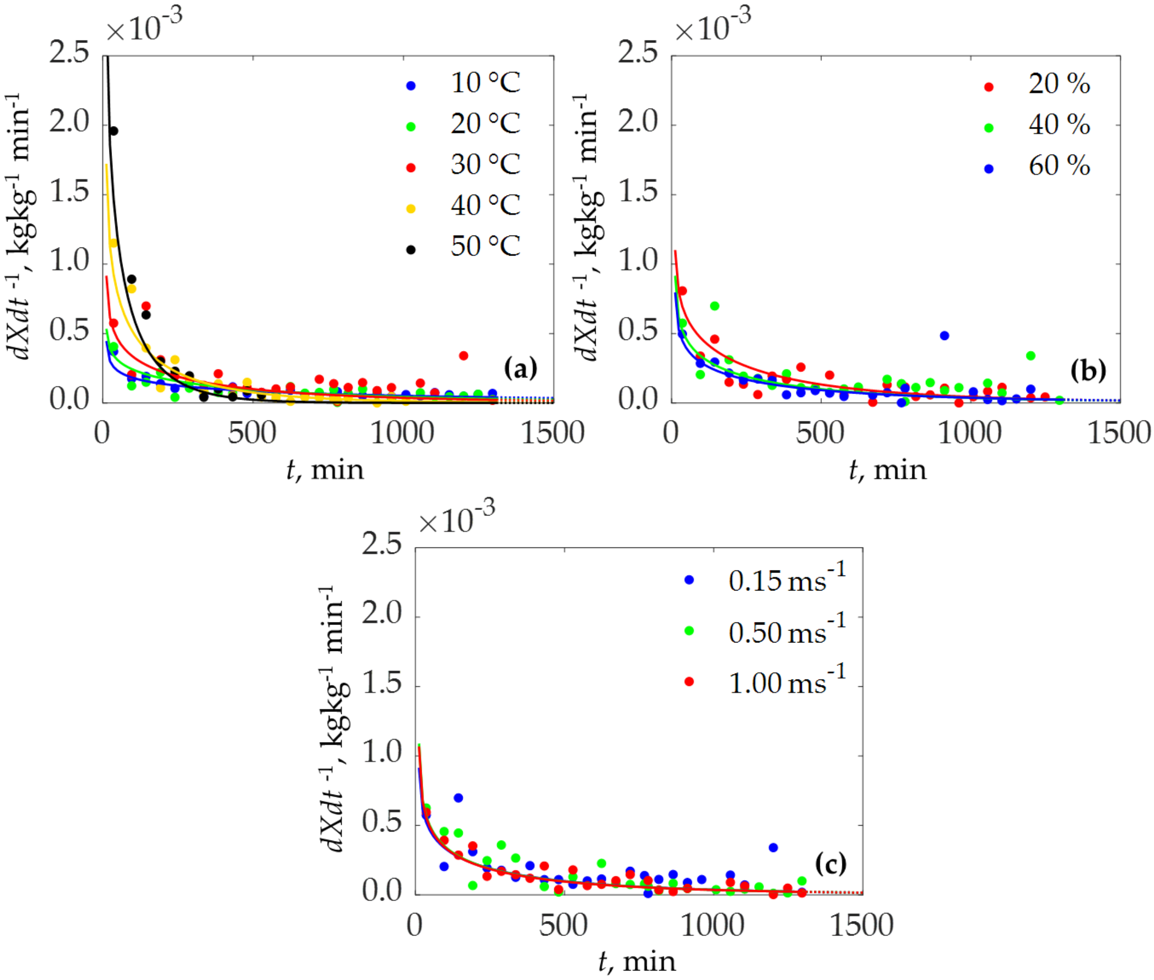

Figure 5. Drying rate $dXdt^{-1}$ vs. time t; (**a**) temperature T ranging from 10 to 50 °C at relative humidity RH = 40%, airflow velocity v = 0.15 ms^{-1}; (**b**) RH ranging from 20 to 60% at T = 30 °C, v = 0.15 ms^{-1}; (**c**) v ranging from 0.15 to 1.00 ms^{-1} at T = 30 °C, RH = 40%. Solid lines represent Page model fitting, dashed lines show extrapolation beyond the dataset used for fitting.

3.4. Generalized Model

For the drying conditions used in this study, a generalized model was developed using the Page model by fixing n and therefore employing k as a single drying parameter. As n value variation was relatively small, a modification was introduced by averaging the n values ($\sum_{i=1}^{N} n/N$) of all drying trials after the first fitting. Once the n value was fixed at the mean value (n = 0.784), the experimental data were fitted again for each drying condition in order to re-adjust the k value. This modification was proposed by Prakash and Siebenmorgen [63] and it was concluded that the model predictability was slightly reduced whereas the complexity of the generalized model was condensed. Hence, a variation of k between 3.660×10^{-3} and 2.998×10^{-2} for T = 10–50 °C, 9.820×10^{-3} and 8.025×10^{-3} for RH = 20–60% and 8.904×10^{-3} and 9.940×10^{-3} for v = 0.15–1.00 ms^{-1} was ascertained accordingly. The perceived drying constants k were modeled based on an Arrhenius-type relationship as affected by the drying air conditions $k = f\ (T, RH, v)$.

$$k = 2.80 \times 10^{-3} \times e^{0.059\ T} \times RH^{-0.139} \times v^{0.025}$$
$$R^2 = 0.989, RMSE = 6.202 \times 10^{-4}, MAPE = 7.4\% \quad (25)$$

The inclusion of Equation (25) in Equation (6) yielded a generalized model able to describe with high accuracy the temporal behavior of moisture ratio X^* (R^2 = 0.997, $RMSE$ = 1.285 × 10^{-2}, $MAPE$ = 6.5%). The resulting course of the drying constant k as a function of temperature T, relative humidity RH, and airflow velocity v is displayed graphically in Figure 6.

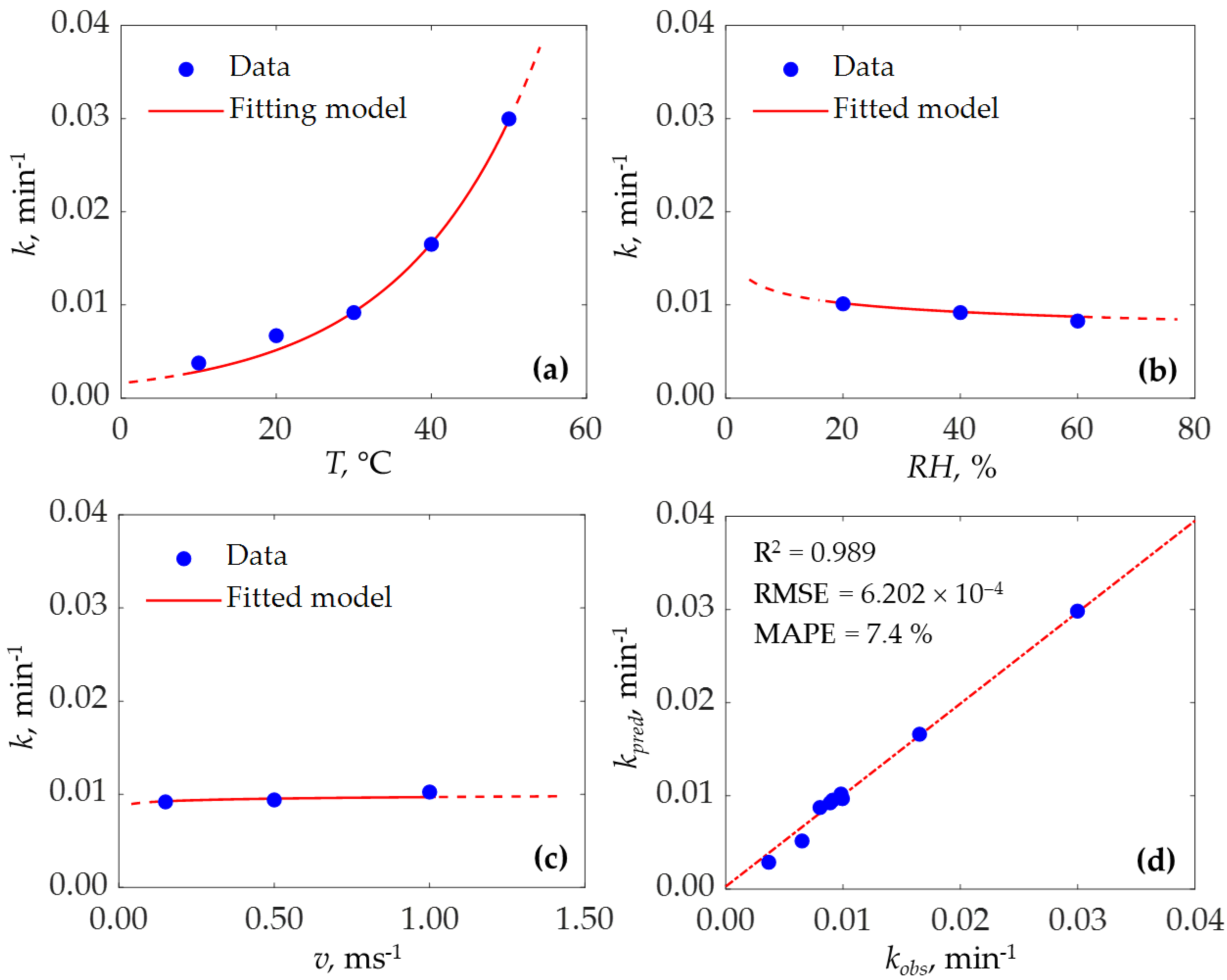

Figure 6. Drying constant k as affected by (**a**) the drying air temperature T, (**b**) relative humidity RH, and (**c**) airflow velocity v. Solid lines represent Page model fitting, dashed lines show extrapolation beyond the dataset used for fitting. (**d**) Predicted values of drying constant k_{pred} vs. observed k_{obs}.

3.5. Effective Moisture Diffusion

Table 3 outlays the values of effective diffusion coefficient D as well as the coefficient of determination, root means square error, and mean absolute percentage error acquired from individual fittings at each drying condition. The statistics confirmed the capability of the short time equation for $1 \leq X^* \leq 0.2$ to predict closely the experimental data at a high accuracy of $R^2 \geq 0.941$, $RMSE \leq 5.595 \times 10^{-2}$ and $MAPE \leq 10.8\%$. From the inspection of Table 3, values of D increased with the increase of T, v and decrease of RH. The values of D varied from 2.474 × 10^{-12} to 3.921 × 10^{-11} for T from 10 to 50 °C, 7.843 × 10^{-11} to 9.822 × 10^{-12} for RH from 20 to 60% and 8.963 × 10^{-12} to 1.063 × 10^{-11} for v from 0.15 to 1.00 ms^{-1}. This can be ascribed to the higher energy of molecules at high T, low RH

and high v, which in turn increases the mobility of molecules, resulting in a faster rate of moisture transfer via diffusion. The derived values of effective diffusion coefficient D are in the similar range with the findings of Gastón, Abalone and Giner [29] and Giner and Mascheroni [30] particularly at $T \geq 30$ °C.

Moreover, the observed values were slightly lower compared to the values reported by Rafiee, Keyhani and Jafari [33] at the same range of drying temperatures which can be attributed to differences in wheat varieties and systems used for drying. However, the effective diffusion coefficient subjected to temperatures lower than 30 °C, as well as various sets of RH and v, has not been studied to date. In an analogy with Equation (25), an analytical model with embodied drying air conditions $D = f\,(T, RH, v)$ was established for describing the effective moisture diffusion coefficients (Equation 26).

$$k = 2.077 \times 10^{-12} \times e^{0.073 \times T} \times RH^{-0.156} \times v^{0.066}$$
$$R^2 = 0.997,\ RMSE = 5.828 \times 10^{-13},\ MAPE = 6.8\% \tag{26}$$

The insertion of Equation (26) in Equation (21) yielded a generalized model based on short time diffusive solution able to depict the drying behavior of wheat cv. 'Pionier' at an accuracy of $R^2 = 0.988$, $RMSE = 4.239 \times 10^{-2}$ and $MAPE = 7.7\%$.

Table 3. Effective moisture diffusion coefficients D for short times ($1 \leq X^* \leq 0.2$) depending on the drying conditions (T, RH, v) and statistical results (R^2, $RMSE$, $MAPE$).

Drying Conditions	D, m^{2}s^{-1}	R^2, –	$RMSE$, –	$MAPE$, %
T10/RH40/V015	2.474×10^{-12}	0.941	3.281×10^{-2}	4.5
T20/RH40/V015	5.811×10^{-12}	0.957	4.403×10^{-2}	9.4
T30/RH40/V015	8.963×10^{-12}	0.956	4.501×10^{-2}	8.2
T40/RH40/V015	1.917×10^{-11}	0.946	5.213×10^{-2}	10.7
T50/RH40/V015	3.921×10^{-11}	0.947	5.595×10^{-2}	10.8
T30/RH20/V015	9.822×10^{-12}	0.956	4.570×10^{-2}	8.6
T30/RH60/V015	7.843×10^{-12}	0.964	4.005×10^{-2}	7.0
T30/RH40/V05	9.494×10^{-12}	0.962	4.186×10^{-2}	7.4
T30/RH40/V1	1.061×10^{-11}	0.959	4.451×10^{-2}	7.8

3.6. Sensitivity Analysis

The sensitivity analysis was performed with the purpose of screening the variance of moisture content attributed to drying conditions (T, RH, v). The general procedure involves the inclusion of Equations (2), (6) and (25) and using Monte Carlo simulation to generate randomized combination of values of drying conditions in order to assess the relation between the inputs and outputs. Figure 7 presents the tornado plot in which parameters are ranked by influence. According to the sensitivity analysis, temperature T is the most significant variable which governs the moisture transport in all cases. A value of −0.799 was observed for the standardized regression coefficient. This means that the increase in temperature T of drying air has a negative effect in moisture content by reducing it. In analogy, values of 0.337 and −0.051 were observed for relative humidity RH and velocity v. Noticeably, drying of wheat can be enhanced by the increase of T, reduction of RH, and increase of v.

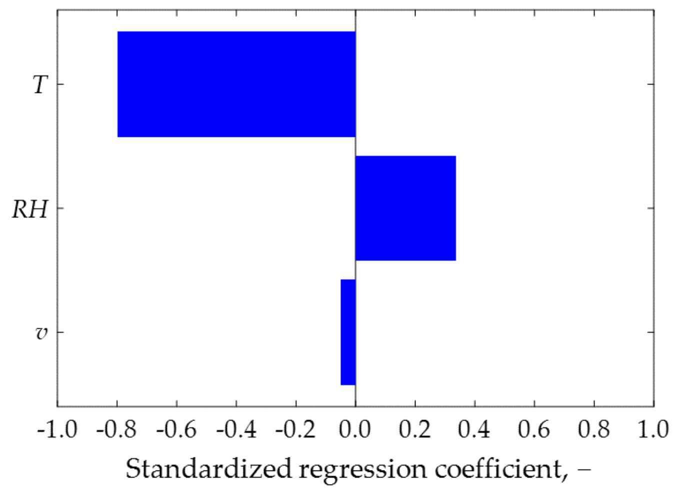

Figure 7. Standardized regression coefficient from sensitivity analysis comprising temperature T, relative humidity RH and airflow velocity v.

4. Conclusions

In this study, the drying kinetics of wheat (*Triticum aestivum* L., cv. 'Pionier') under a coherent set of low-temperature drying conditions were investigated. A robust and automated measurement system using a high precision balance was employed as the basis for the real-time and continuous acquisition of drying data. Drying experiments revealed that temperature T of drying air had the greatest influence on the drying behavior for the specified range of applicability followed by relative humidity RH and velocity v. Moreover, the applications of low temperatures for cooling, aeration and drying entailed a slow and gentle drying process due to the low water-uptake capacity as compared to drying with high temperatures. For the characterization of drying behavior, several semi-empirical models were employed, out of which Page model was found favorable to fit the experimental data based on statistical indicators. A generalized model for low-temperature drying with drying constant k ranging from 3.660×10^{-3} to 2.998×10^{-2} was established, which demonstrated a great potential to portray the drying behavior of wheat with a high accuracy (R^2 = 0.997, $RMSE$ = 1.285×10^{-2}, $MAPE$ = 6.5%). The temperature T, relative humidity RH and velocity v of the drying air were embodied in the generalized model framework. Furthermore, an analytical approach for predicting the effective diffusion coefficients was established based on short time diffusive solution (R^2 = 0.988, $RMSE$ = 4.239×10^{-2}, $MAPE$ = 7.7%). A variation of effective diffusion coefficient from 2.474×10^{-12} to 4.494×10^{-11} was ascertained for the applied drying conditions (T = 10–50 °C, RH = 20–60% and v = 0.15–1.00 ms^{-1}).

The developed drying model can be employed in the design, modeling and optimization of cooling, aeration and low-temperature drying processes of wheat bulks, which apply the alike range of air conditions. Further investigations should embrace the assessment of nutritional and structural changes of wheat during the long drying times required for low-temperature drying. In addition, the evaluation of energy efficiency as compared to high-temperature drying methods needs to be investigated in further studies.

Author Contributions: Conceptualization, I.R., S.S. and J.M.; methodology, I.R., S.S. and J.M.; software, I.R.; validation, I.R.; formal analysis, I.R., S.S. and J.M.; investigation, I.R.; resources, I.R. and J.M.; data curation, I.R.; writing—original draft preparation, I.R.; writing—review and editing, I.R., S.S. and J.M.; visualization, I.R.; supervision, J.M.; project administration, I.R., S.S. and J.M.; funding acquisition, J.M. All authors have read and agreed to the published version of the manuscript.

Funding: This research was financially supported by the German Federal Ministry for Economic Affairs and Energy (BMWi), in the framework of the "Zentrales Innovationsprogramm Mittelstand (ZIM)" with project number KF2607404LT4.

Institutional Review Board Statement: Not applicable.

Informed Consent Statement: Not applicable.

Data Availability Statement: Not applicable.

Conflicts of Interest: The authors declare no conflict of interest.

Nomenclature

α_v	Kernel-specific surface area, m^2m^{-3}
A_0, A_1	Coefficients of drying model, –
C_1, C_2, C_3	Coefficients of sorption isotherm model, –
D	Effective moisture diffusion coefficient, m^2s^{-1}
d	Diameter of sample holder, mm
h	Height of sample holder, mm
d.b.	Dry basis, –
k	Drying constant, min^{-1}
k_{pred}	Predicted drying constant, min^{-1}
k_{obs}	Observed drying constant, min^{-1}
$MAPE$	Mean absolute percentage error, %
N	Number of observations, –
n	Drying model coefficient, –
p	Probability level, –
R^2	Coefficient of determination, –
R_e	Equivalent radius of wheat kernel, m
RH	Relative humidity of drying air, %
T	Temperature of drying air, °C
v	Airflow velocity of drying air, ms^{-1}
w.b.	Wet basis, %
X^*	Moisture ratio, –
X^*_{pred}	Predicted moisture ratio, –
X^*_{obs}	Observed moisture ratio, –
X_0	Initial moisture content, kg kg^{-1} d.b.
X_{eq}	Equilibrium moisture content, kg kg^{-1} d.b.
X_t	Instantaneous moisture content, kg kg^{-1} d.b.
X_{pred}	Predicted moisture content, kg kg^{-1} d.b.
X_{obs}	Observed moisture content, kg kg^{-1} d.b.
t	Drying time, min
t_0	Initial drying time, min
Δt	Drying time interval, min

Appendix A

Table A1. The experimental mean values of equilibrium moisture content X_{eq} and standard deviations for all sets of temperatures T and relative humidity RH observed from the gravimetric salt method.

***T* = 10 °C**		***T* = 30 °C**		***T* = 50 °C**	
RH, %	X_{eq}, kg kg^{-1} *d.b.*	*RH*, %	X_{eq}, kg kg^{-1} *d.b.*	*RH*, %	X_{eq}, kg kg^{-1} *d.b.*
12.3	0.056 ± 0.001	7.4	0.036 ± 0.001	5.7	0.023 ± 0.001
23.4	0.081 ± 0.001	21.6	0.063 ± 0.005	18.9	0.041 ± 0.010
33.5	0.105 ± 0.001	32.4	0.097 ± 0.001	30.5	0.082 ± 0.002
44.1	0.129 ± 0.019	43.2	0.103 ± 0.001	42.7	0.084 ± 0.001
62.2	0.146 ± 0.001	56.0	0.123 ± 0.003	50.9	0.095 ± 0.000
72.1	0.168 ± 0.001	68.9	0.147 ± 0.001	65.3	0.118 ± 0.001
75.7	0.179 ± 0.001	75.3	0.165 ± 0.001	74.5	0.138 ± 0.004
86.8	0.217 ± 0.001	83.6	0.194 ± 0.002	81.2	0.164 ± 0.010

References

1. FAO. Food and Agriculture Data. Available online: http://www.fao.org/faostat/en/#data (accessed on 12 June 2021).
2. Watson, R.R.; Preedy, V.R.; Zibadi, S. *Wheat and Rice in Disease Prevention and Health: Benefits, Risks and Mechanisms of Whole Grains in Health Promotion*; Academic Press: Cambridge, MA, USA, 2014.
3. Saini, P.; Kumar, N.; Kumar, S.; Mwaurah, P.W.; Panghal, A.; Attkan, A.K.; Singh, V.K.; Garg, M.K.; Singh, V. Bioactive compounds, nutritional benefits and food applications of colored wheat: A comprehensive review. *Crit. Rev. Food Sci. Nutr.* **2020**, *16*, 1–14. [CrossRef]
4. Navarro, S.; Noyes, R.T. *The Mechanics and Physics of Modern Grain Aeration Management*; CRC Press: Boca Raton, FL, USA, 2001.
5. Magan, N.; Aldred, D.; Mylona, K.; Lambert, R.J.W. Limiting mycotoxins in stored wheat. *Food Addit. Contam.-Part A Chem. Anal. Control. Expo. Risk Assess.* **2010**, *27*, 644–650. [CrossRef] [PubMed]
6. Thorpe, G.R. The modelling and potential applications of a simple solar regenerated grain cooling device. *Postharvest Biol. Technol.* **1998**, *13*, 151–168. [CrossRef]
7. Maier, D.; Navarro, S. Chilling of grain by refrigerated air. In *The Mechanics and Physics of Modern Grain Aeration Management*; CRC Press: Boca Raton, FL, USA, 2002; pp. 489–560.
8. Mühlbauer, W. *Handbuch der Getreidetrocknung: Grundlagen und Verfahren*; Agrimedia: Clenze, Germany, 2009.
9. Mühlbauer, W.; Müller, J. Chapter 3.6-Wheat (*Triticum* L.). In *Drying Atlas*; Mühlbauer, W., Müller, J., Eds.; Woodhead Publishing: Sawston, UK, 2020; pp. 109–115.
10. Ileleji, K.E.; Maier, D.E.; Woloshuk, C.P. Evaluation of different temperature management strategies for suppression of *Sitophilus zeamais* (Motschulsky) in stored maize. *J. Stored Prod. Res.* **2007**, *43*, 480–488. [CrossRef]
11. Bala, B.K. *Drying and Storage of Cereal Grains*; John Wiley & Sons: Hoboken, NJ, USA, 2016.
12. Sharp, J.R. A review of low temperature drying simulation models. *J. Agric. Eng. Res.* **1982**, *27*, 169–190. [CrossRef]
13. Nagaya, K.; Li, Y.; Jin, Z.; Fukumuro, M.; Ando, Y.; Akaishi, A. Low-temperature desiccant-based food drying system with airflow and temperature control. *J. Food Eng.* **2006**, *75*, 71–77. [CrossRef]
14. Ondier, G.O.; Siebenmorgen, T.J.; Mauromoustakos, A. Low-temperature, low-relative humidity drying of rough rice. *J. Food Eng.* **2010**, *100*, 545–550. [CrossRef]
15. Venkatachalam, S.K.; Thottipalayam Vellingri, A.; Selvaraj, V. Low-temperature drying characteristics of mint leaves in a continuous-dehumidified air drying system. *J. Food Process. Eng.* **2020**, *43*, e13384. [CrossRef]
16. Onwude, D.I.; Hashim, N.; Chen, G. Recent advances of novel thermal combined hot air drying of agricultural crops. *Trends Food Sci. Technol.* **2016**, *57*, 132–145. [CrossRef]
17. El-Sebaii, A.A.; Shalaby, S.M. Solar drying of agricultural products: A review. *Renew. Sustain. Energy Rev.* **2012**, *16*, 37–43. [CrossRef]
18. Bruce, D.M. A model of the effect of heated-air drying on the bread baking quality of wheat. *J. Agric. Eng. Res.* **1992**, *52*, 53–76. [CrossRef]
19. Giner, S.A.; Calvelo, A. Modelling of Wheat Drying in Fluidized Beds. *J. Food Sci.* **1987**, *52*, 1358–1363. [CrossRef]
20. Nellist, M.E. Modelling the performance of a cross-flow grain drier. *J. Agric. Eng. Res.* **1987**, *37*, 43–57. [CrossRef]
21. Mellmann, J.; Richter, I.G.; Maltry, W. Experiments on Hot-Air Drying of Wheat in a Semi-Technical Mixed-Flow Dryer. *Dry. Technol.* **2007**, *25*, 1287–1295. [CrossRef]
22. Lupano, C.; Añón, M. Denaturation of wheat germ proteins during drying. *Cereal Chem.* **1986**, *63*, 259–262.
23. Bhullar, S.; Jenner, C. Differential responses to high temperatures of starch and nitrogen accumulation in the grain of four cultivars of wheat. *Funct. Plant Biol.* **1985**, *12*, 363–375. [CrossRef]
24. Mis, A.; Grundas, S. Influence of the moistening and drying of wheat grain on its hardness. *Int. Agrophys.* **2004**, *18*, 47–53.
25. Glenn, G.M.; Younce, F.L.; Pitts, M.J. Fundamental physical properties characterizing the hardness of wheat endosperm. *J. Cereal Sci.* **1991**, *13*, 179–194. [CrossRef]
26. Cubadda, R.E.; Carcea, M.; Marconi, E.; Trivisonno, M.C. Influence of Gluten Proteins and Drying Temperature on the Cooking Quality of Durum Wheat Pasta. *Cereal Chem.* **2007**, *84*, 48–55. [CrossRef]
27. Dexter, J.E.; Matsuo, R.R.; Morgan, B.C. High Temperature Drying: Effect on Spaghetti Properties. *J. Food Sci.* **1981**, *46*, 1741–1746. [CrossRef]
28. D'Amico, S.; Mäschle, J.; Jekle, M.; Tömösközi, S.; Langó, B.; Schoenlechner, R. Effect of high temperature drying on gluten-free pasta properties. *LWT-Food Sci. Technol.* **2015**, *63*, 391–399. [CrossRef]
29. Gastón, A.a.L.; Abalone, R.M.; Giner, S.A. Wheat drying kinetics. Diffusivities for sphere and ellipsoid by finite elements. *J. Food Eng.* **2002**, *52*, 313–322. [CrossRef]
30. Giner, S.; Mascheroni, R. PH—Postharvest Technology: Diffusive Drying Kinetics in Wheat, Part 2: Applying the Simplified Analytical Solution to Experimental Data. *Biosyst. Eng.* **2002**, *81*, 85–97. [CrossRef]
31. Hemis, M.; Bettahar, A.; Singh, C.B.; Bruneau, D.; Jayas, D.S. An Experimental Study of Wheat Drying in Thin Layer and Mathematical Simulation of a Fixed-Bed Convective Dryer. *Dry. Technol.* **2009**, *27*, 1142–1151. [CrossRef]
32. Mohapatra, D.; Srinivasa Rao, P. A thin layer drying model of parboiled wheat. *J. Food Eng.* **2005**, *66*, 513–518. [CrossRef]
33. Rafiee, S.; Keyhani, A.; Jafari, A. Modeling Effective Moisture Diffusivity of Wheat (Tajan) During Air Drying. *Int. J. Food Prop.* **2008**, *11*, 223–232. [CrossRef]
34. Watson, E.; Bhargava, V. Thin-layer drying studies on wheat. *Can. Agric. Eng.* **1974**, *16*, 18–22.

35. Argyropoulos, D.; Heindl, A.; Müller, J. Assessment of convection, hot-air combined with microwave-vacuum and freeze-drying methods for mushrooms with regard to product quality. *Int. J. Food Sci. Technol.* **2011**, *46*, 333–342. [CrossRef]
36. Munder, S.; Argyropoulos, D.; Müller, J. Acquisition of Sorption and Drying Data with Embedded Devices: Improving Standard Models for High Oleic Sunflower Seeds by Continuous Measurements in Dynamic Systems. *Agriculture* **2019**, *9*, 1. [CrossRef]
37. Sinicio, R.; Muir, W.E.; Jayas, D.S.; Cenkowski, S. Thin-layer drying and wetting of wheat. *Postharvest Biol. Technol.* **1995**, *5*, 261–275. [CrossRef]
38. Sokhansanj, S.; Singh, D.; Wasserman, J. Drying Characteristics of Wheat, Barley and Canola Subjected to Repetitive Wetting and Drying Cycles. *Trans. ASAE* **1984**, *27*, 903–0906. [CrossRef]
39. Cao, C.; Yu, W. Thin layer drying studies on wheat. *J. Beijing Agric. Eng. Univ.* **1987**, *7*, 47–54.
40. O'callaghan, J.; Menzies, D.; Bailey, P. Digital simulation of agricultural drier performance. *J. Agric. Eng. Res.* **1971**, *16*, 223–244. [CrossRef]
41. Nishiyama, Y. Grain drying simulation by the sphere drying model. Proceedings of 4th International Drying Symposium, Kyoto, Japan, 9–12 July 1984; pp. 513–519.
42. Singh, D.; Sokhansanj, S.; Middleton, B. *Drying Characteristics of Wheat, Barley and Canola at Low Temperatures*; ASAE Paper No. NCR 83207; ASAE: St. Joseph, MI, USA, 1983.
43. Karaj, S.; Müller, J. Determination of physical, mechanical and chemical properties of seeds and kernels of *Jatropha curcas* L. *Ind. Crop. Prod.* **2010**, *32*, 129–138. [CrossRef]
44. AOAC. *Official Methods of Analysis*, 16th ed.; Association of Analytical Chemist: Arlington, VA, USA, 1998.
45. Nimkar, P.M.; Chattopadhyay, P.K. PH—Postharvest Technology: Some Physical Properties of Green Gram. *J. Agric. Eng. Res.* **2001**, *80*, 183–189. [CrossRef]
46. Sacilik, K.; Öztürk, R.; Keskin, R. Some Physical Properties of Hemp Seed. *Biosyst. Eng.* **2003**, *86*, 191–198. [CrossRef]
47. Reyer, S.; Awiszus, S.; Meissner, K.; Müller, J. High precision laboratory dryer for thin layer and bulk drying with adjustable temperature, relative humidity and velocity of the drying air. *HardwareX* **2020**, *8*, e00133. [CrossRef]
48. Udomkun, P.; Argyropoulos, D.; Nagle, M.; Mahayothee, B.; Müller, J. Sorption behaviour of papayas as affected by compositional and structural alterations from osmotic pretreatment and drying. *J. Food Eng.* **2015**, *157*, 14–23. [CrossRef]
49. Lewis, W.K. The Rate of Drying of Solid Materials. *J. Ind. Eng. Chem.* **1921**, *13*, 427–432. [CrossRef]
50. Page, G.E. *Factors Influencing the Maximum Rates of Air Drying Shelled Corn in Thin Layers*; Purdue University: West Lafayette, IN, USA, 1949.
51. Henderson, S.M. Grain drying theory (I) temperature effect on drying coefficient. *J. Agric. Eng. Res.* **1961**, *6*, 169–174.
52. Chandra, P.K.; Singh, R.P. *Applied Numerical Methods for Food and Agricultural Engineers*; CRC Press: Boca Raton, FL, USA, 1994.
53. Midilli, A.; Kucuk, H.; Yapar, Z. A new model for single-layer drying. *Dry. Technol.* **2002**, *20*, 1503–1513. [CrossRef]
54. Guillard, V.; Bourlieu, C.; Gontard, N. *Food Structure and Moisture Transfer: A Modeling Approach*; Springer Science & Business Media: Berlin, Germany, 2013.
55. Erbay, Z.; Icier, F. A review of thin layer drying of foods: Theory, modeling, and experimental results. *Crit. Rev. Food Sci. Nutr.* **2010**, *50*, 441–464. [CrossRef]
56. Ertekin, C.; Firat, M.Z. A comprehensive review of thin-layer drying models used in agricultural products. *Crit. Rev. Food Sci. Nutr.* **2017**, *57*, 701–717. [CrossRef] [PubMed]
57. Udomkun, P.; Argyropoulos, D.; Nagle, M.; Mahayothee, B.; Janjai, S.; Müller, J. Single layer drying kinetics of papaya amidst vertical and horizontal airflow. *LWT-Food Sci. Technol.* **2015**, *64*, 67–73. [CrossRef]
58. Hui, Y.H. *Food Drying Science and Technology: Microbiology, Chemistry, Applications*; DEStech Publications, Inc.: Lancaster, PA, USA, 2008.
59. Giner, S.A.; Mascheroni, R.H. PH—Postharvest Technology: Diffusive Drying Kinetics in Wheat, Part 1: Potential for a Simplified Analytical Solution. *J. Agric. Eng. Res.* **2001**, *80*, 351–364. [CrossRef]
60. Sun, D.W.; Woods, J.L. The selection of sorption isotherm equations for wheat based on the fitting of available data. *J. Stored Prod. Res.* **1994**, *30*, 27–43. [CrossRef]
61. Brunauer, S. *The Adsorption of Gases and Vapors Vol I—Physical Adsorption*; Princeton University Press: Princeton, NJ, USA, 1943.
62. Jayas, D.; Sokhansanj, S. Thin-layer drying of wheat at low temperatures. *Drying* **1986**, *86*, 844–847.
63. Prakash, B.; Siebenmorgen, T.J. Single-Parameter Thin-Layer Drying Equations for Long-Grain Rice. *Trans. ASABE* **2018**, *61*, 733–742. [CrossRef]